Influence of geometry on current-driven vortex oscillations in nanocontact devices

E. Jaromirska,[1] L. Lopez-Diaz,[1] A. Ruotolo,[2,3] J. Grollier,[2] V. Cros,[2] and D. Berkov[4]
[1]*Departamento de Física Aplicada, Universidad de Salamanca, Spain*
[2]*Unité Mixte de Physique CNRS/Thales and Université Paris Sud 11, France*
[3]*Department of Physics and Materials Science, City University of Hong Kong, Kowloon, Hong Kong*
[4]*Innovent Technology Development e.V., Jena, Germany*
(Received 22 October 2010; revised manuscript received 8 February 2011; published 16 March 2011)

We present a computational study of current-driven vortex dynamics in a particular geometry, a hybrid Co/Au/Py nanocontact, in which the Co layer is not flat. The experimental measurements validate the numerical results. We identify the Py layer as dynamically active. The nonuniform magnetization configuration in the Co layer, which acts as spin polarizer, and the interlayer magnetostatic stray field, both of which are mostly determined by geometry, are shown to have crucial influence on the dynamic properties of the system. The frequency as a function of current at zero field and also as a function of an out-of-plane field for a fixed current are computed. An excellent quantitative agreement with experimental data is obtained, demonstrating a novel approach for tailoring vortex nano-oscillators.

DOI: 10.1103/PhysRevB.83.094419 PACS number(s): 75.78.Cd

I. INTRODUCTION

It is now well established that when a spin-polarized current flows through a ferromagnetic conductor it exerts a torque on the local magnetic moments.[1–3] In multilayered systems (magnetoresistive spin valves or tunnel junctions) this phenomenon can lead to novel effects, such as current-induced magnetization reversal[2,4] or self-sustained microwave oscillations,[5,6] which have been investigated extensively over the last years. The latter brings about some promising possibilities for designing a new type of nanoscale oscillator, the so-called spin-transfer nano-oscillator (hereafter STNO).

In most of the experiments up to now, current induced coherent excitations were built upon a quasi-uniform equilibrium state.[5,6] Recently, however, it has been shown that spin torque (ST) can also excite precessional motion of magnetic vortex in metallic nanopillars,[7] nanocontacts[8,9] and magnetic tunnel junctions.[10] Vortex excitations[11] are interesting not only from a fundamental point of view, but also because they present some desirable properties for applications in telecommunication devices, that is, sub-GHz linewidths and the possibility to operate at low or even without external field.

In pillar geometry, due to the lateral confinement, when vortex is displaced from the center magnetic charges appear at the lateral surface increasing the dipolar stray field energy of the system and, therefore, a position-dependent potential is created leading to vortex oscillations around its central (equilibrium) position. This is the well-known rotational vortex mode, which has been studied theoretically[12] and detected experimentally.[11] The excitation of vortex dynamics, and in particular of the rotational mode, by a current-perpendicular-to-plane spin-polarized current has been recently investigated both theoretically[13–16] and experimentally.[7,10,17]

On the contrary, in nanocontact geometry, where the lateral confinement does not exist at all, the vortex energy is, in principle, independent of the position. However, when current is passed through the nanocontact, the associated Oersted field can nucleate a vortex. In the created attractive potential the minimum energy corresponds to the vortex centered at the contact. Thus, in the presence of spin-polarized current, the vortex might orbit around the nanocontact and these oscillations persist in time if the ST counterbalances energy dissipation in the system.

This new vortex rotational mode has been recently identified and measured experimentally in metallic nanocontacts.[8,9,18,19] It is characterized by a large-amplitude signal of low frequency (100–600 MHz) that increases linearly with current at a small rate ($\frac{df}{dI} \sim 10$ MHz/mA) and that weakly depends on the magnitude of the in-plane field as long as it does not exceed a certain value (typically a few mT).

Although this mode was initially found only for substantial ($B > 0.1$ T) out-of-plane fields,[8,9] recently it has been shown that vortex oscillations can also be sustained at zero field.[18–21] A rigid vortex model based on a more general Thiele's equation[22] was used to explain the basic mechanism for this mode as it successfully describes some basic trends, such as the linear frequency blueshift with current and the frequency decrease with the magnitude of the out-of-plane field at large fields.[9] In this model, a spin polarization perpendicular to the film plane is necessary to maintain vortex oscillations.[9] Therefore, it cannot explain vortex oscillations at zero field, since the perpendicular polarization is expected to be negligibly small in this case. This model was recently generalized[23] to include the ST coming from in-plane currents and it was shown that this term could support vortex oscillations in the absence of an external field. On the other hand, using a slightly different model it was shown that, in a pillar geometry, a nonuniform in-plane polarizer could also be responsible for sustaining vortex oscillations.[24] In any case, the predictions of both models have not been tested by direct comparison with experimental data and the mechanism driving vortex oscillations without external field needs to be investigated further.

In the present work we use micromagnetic simulations to show that, in our particular system, zero-field vortex oscillations appear as a consequence of the combined action of a nonuniform spin polarization and the stray field from the polarizing layer, both of which are mostly determined by the geometry of the device. The system under study is

a Co (15 nm)/Au (6 nm)/Py (4 nm) nanocontact with a local constriction in the Co layer. A detailed investigation of vortex oscillations in this system is presented. We demonstrate how the nonflat profile of the Co layer influences the current distribution, the associated Oersted field, and the interlayer dipolar stray field. These are shown to have crucial impact on the dynamic properties of the studied STNO, such as spectra with multiharmonics, tunability and dependence on the external field. The results are compared to experimental data yielding excellent quantitative agreement.

The paper is organized as follows. Some specifications and technical details about the simulations are given in Sec. II. In Sec. III vortex oscillations in the absence of an external field are discussed. Section IV addresses the impact of an out-of-plane field on the vortex orbit and frequency. Final conclusions are highlighted in Sec. V.

II. SIMULATION SPECIFICATIONS

The system under study, which is schematically represented in Fig. 1, has been chosen to mimic as closely as possible a real sample in order to be able to compare the predictions of our simulations to experimental data. The real sample is a sputtered multilayer with composition Ta (5 nm)/Cu (40 nm)/Py (4 nm)/Au (6 nm)/Co (15 nm)/Au (100 nm). A nanocontact of nominal diameter of 20 nm was opened by conductive tip atomic microscope nanoindentation and plasma etching, the details of which can be found elsewhere.[25] As a result, a nonflat locally (in the vicinity of the nanocontact) constrained Co layer was obtained, which is modeled as an inverted truncated cone with upper and lower radii of 100 and 15 nm, respectively. This yields inclination of 25° with respect to the horizontal plane (Fig. 1). This geometry is referred to as the hybrid geometry hereafter.

The micromagnetic simulations in the ST trilayer were carried out using OOMMF.[26] A circular region of 2.5 μm in diameter was considered, which is large enough to guarantee that the vortex dynamics is not affected by the boundaries. Thus, a $2500 \times 2500 \times 65$ nm^3 system was discretized into $5 \times 5 \times 2.5$ nm^3 cells. The following values for the saturation magnetization and exchange constant were chosen for the ferromagnetic layers: $M_{s,Py} = 0.6 \times 10^6$ A/m, $M_{s,Co} = 1.4 \times 10^6$ A/m, $A_{Py} = 1.4 \times 10^{-11}$ J/m, $A_{Co} = 3.0 \times 10^{-11}$ J/m. No magneto-crystalline anisotropy was considered in Py

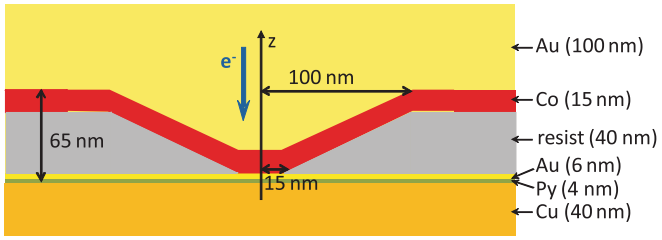

FIG. 1. (Color online) Schematic representation of the system under study. A cross section through the middle plane is represented. The bottom and the top electrodes are 40-nm Cu and 100-nm Au layers, respectively. In between, the Py (4 nm)/Au (6 nm)/Co (15 nm) represents the ST trilayer, which includes the contact opened on top of the 40-nm resist layer. Positive current direction corresponds to electrons flowing from the Co to the Py layer.

or in Co and thermal fluctuations were not taken into account. For the current-driven simulations, in which only the dynamics in the Py layer is resolved, the computational region was discretized into $5 \times 5 \times 4$ nm^3 cells. The ST term acting on the magnetization of the Py layer is given by $\Gamma_{ST} = \frac{\gamma \hbar J P}{2|e|t} \mathbf{m} \times (\mathbf{m} \times \mathbf{m}_p)$, where γ is the gyromagnetic ratio, J is the current density, P is the polarization factor, t is the thickness of the Py layer, and $\mathbf{m}$ and $\mathbf{m_p}$ are the normalized magnetizations in the Py and Co layers, respectively.

In this hybrid geometry it is expected that the nonflat Co layer strongly influences the current distribution and the associated Oersted field. Therefore, the commonly used simplifying assumptions of uniform current distribution across the nanocontact and Oersted field as approximated by the infinite straight conductor are not accurate in this case. Thus, both mentioned distributions have been calculated using a finite element electromagnetic solver[27] and incorporated into micromagnetic simulations. The following values for the resistivity of the materials involved have been used: $\rho_{Cu} = 1.7 \times 10^{-8}\,\Omega$ m, $\rho_{Au} = 2.5 \times 10^{-8}\,\Omega$ m, $\rho_{Py} = 7.0 \times 10^{-8}\,\Omega$ m, $\rho_{Co} = 7.0 \times 10^{-8}\,\Omega$ m.

The arrow plot of the calculated current density distribution is shown in Fig. 2, where (a) and (b) represent color plots of the current density magnitude in the nanocontact cross-section region in the Co and Py layers, respectively. Through the nanocontact the current flows mostly perpendicular to the film plane but in the inclined region in the Co layer significant in-plane currents are present. The cross-sectional density plot at the level of Co [Fig. 2(a)] reveals that significantly larger current density is found at the edges rather than in the central region of the nanocontact. The calculated distribution becomes more uniform below the contact in the Py layer [Fig. 2(b)].

On the other hand, the calculated Oersted field profile as a function of distance from the nanocontact center is represented at different levels in the main panel of Fig. 3. In the inset, a color plot of the field strength is presented indicating the position of the above-mentioned levels. The analytical profile obtained assuming that the current flows uniformly through an infinite conductor of radius R_{PC} is also shown (solid black squares). It increases linearly inside the nanocontact and decays as $1/r$ outside. As it can be seen, the maximum of the Oersted field is smaller than the analytical prediction and it is shifted outside the nanocontact due to the current spreading. We also point out that in the top part of the Co layer (blue inverted triangles) the Oersted field is much weaker than at the contact level itself (red circles). Moreover, on the top of the nanocontact (green triangles) the maximum Oersted field is approximately half the value directly at the contact level. These features are relevant in the discussion that follows.

Additionally, comparing current and Oersted distributions in flat and hybrid structures we conclude that it is the presence of the constriction in the latter that is responsible for the appearance of the features listed above. Thus, the results are general for structures where inclination angle is significant, that is, fabricated by nanoindentation technique. Different behavior is observed in flat structures where the contact is opened for example by wet etching.

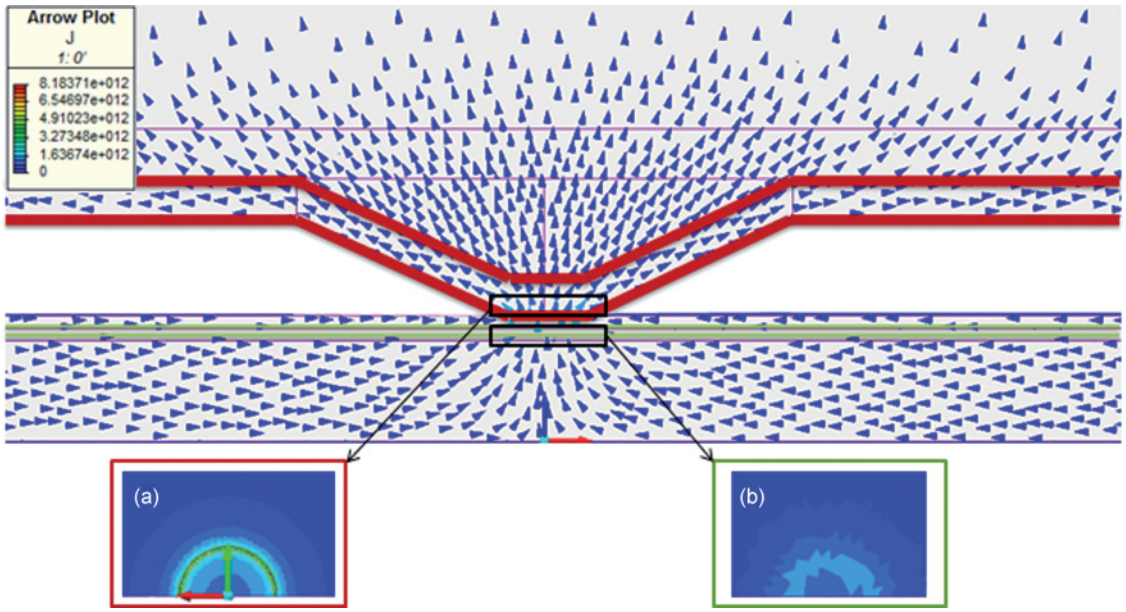

FIG. 2. (Color online) Arrow plot of the current density $\vec{J}(\vec{r})$ for a total current $I = 1$ mA. The arrows point along the positive current direction (electron flow is along the opposite direction). Color plot of the current density in (a) the Co layer and (b) the Py layer at the nanocontact.

III. OSCILLATIONS IN ABSENCE OF EXTERNAL FIELD

Given the specific features of the device geometry and taking into account that none of the two ferromagnetic layers is exchanged biased, it is not straightforward to predict what is the initial magnetization configuration in each layer and which one, if not both of them, is active when the current is applied. In order to clarify this point, we start by investigating possible favorable magnetization configurations in both Co and Py layers before the current is applied. Starting with the system saturated in the positive z direction (Fig. 1) we observe that, due to the lateral constraint imposed by the truncated cone geometry, stray field favors vortex formation in the Co and Py layers, both of them with positive polarity but opposite chiralities, thus minimizing the total stray-field energy.[28] In the experimental data that will be presented later on, however, the presence of two vortices in the system before the current is passed is excluded, since the voltage signal indicates in-plane quasiuniform parallel configuration in both layers.

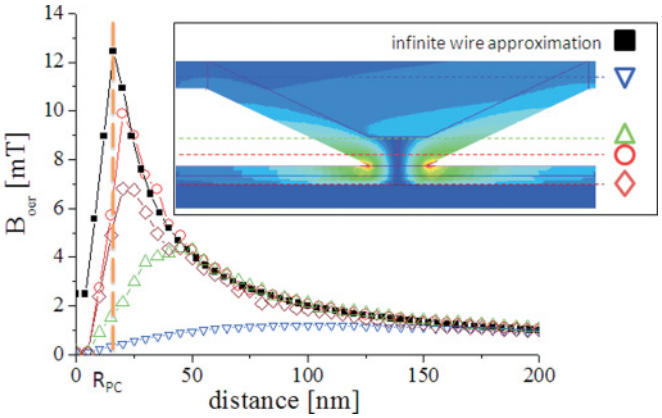

FIG. 3. (Color online) Strength of the Oersted field for a total current $I = 1$ mA as a function of the distance from the nanocontact center in the Py layer (purple diamonds), at the bottom of the Co layer (red circles), at the top of the contact area (green triangles), and in the flat part of the Co layer (blue inverted triangles). The field corresponding to an infinitely long straight wire of radius R_{PC} is shown (black squares) for comparison. The nanocontact radius R_{PC} is marked with the dashed vertical line. (Inset) Color plot of the Oersted field strength showing also the positions of planes corresponding to the field profiles from the main graph.

In a second simulation, starting also from the saturated state, the Oersted field, as calculated in the previous section, was accounted for. As a result, at the current of 10 mA, in the Py layer, a counterclockwise (ccw) vortex is developed (Fig. 4) following the chirality of the Oersted field. A second vortex is formed in the Co layer, but with opposite chirality, as it was the case when the Oersted field was not included. This situation arises because interlayer magnetostatic interaction, which favors vortices with opposite chiralities,[28] dominates over the effect of the Oersted field in Co, which favors ccw chirality. Note that, as it was pointed out in Sec. II, the Oersted field in the Co layer significantly reduces as one moves up along the z coordinate (Fig. 3). After the vortex with clockwise (cw) chirality is nucleated in the Co layer, it is expelled far from the nanocontact area to the top flat part because of the presence of the ccw Oersted field. As a result, a quasiuniform in-plane magnetization configuration is found in the nanocontact area with significant inhomogeneous out-of-plane components of opposite sign at both sides [Figs. 4(b) and 4(c)]. We do not claim that the dynamic evolution predicted by this simulation, which did not include the effect of ST, coincides with the processes taking place in the real system when the current is applied. Certainly, the mechanisms for vortex nucleation in nanocontact devices are complex[29] and their study is beyond the scope of this work. However, the simulations clearly indicate that a vortex with ccw chirality is more easily

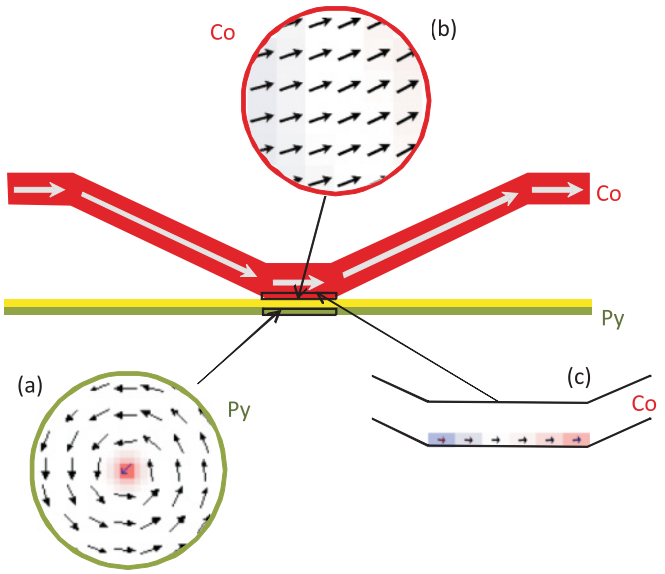

FIG. 4. (Color online) Equilibrium configuration in the system under the action of the Oersted field for the current of $I = 10$ mA. (a) Counterclockwise vortex in Py. (b) Top and (c) side views of the magnetization configuration in the Co layer. In all cases the color scale corresponds to the perpendicular component of the magnetization, where red, blue, and white mean $z > 0$, $z < 0$, and $z = 0$, respectively.

nucleated in the Py than in the Co layer. Considering that the experimental results shown later are compatible with the existence of only one vortex in the system, we conclude that the vortex with ccw chirality is in Py, which is identified as the active layer. On the other hand, the Co layer, which acts as polarizer, remains in the configuration discussed above. Even though the processes taking place in the Co layer could be different, the final magnetization configuration is very likely to be similar to the one found in our simulation, since the out-of-plane profile is determined by the geometry, that is, the slope in the vicinity of the nanocontact, whereas the curling in the in-plane component is determined by the Oersted field.

Consequently, we proceed with the micromagnetic simulations studying the dynamics of the vortex in the Py layer including the ST and assuming that the Co layer is magnetized as shown in Figs. 4(b) and 4(c). To evaluate the ST acting on Py we use a local model in which the current density $J(r)$ at each cell is given by the module of the local current density as calculated in Sec. II, whereas the spin polarization profile is given by the magnetization configuration at the bottom slice of the Co layer. The magnetization configuration in Co not only determines the spin polarization of the current, but it is also the source of a stray field that acts on Py, as shown schematically in Fig. 5(a). This field has been calculated micromagnetically and is presented in the cross-section corresponding to the Py layer in Fig. 5(b). The arrows represent the in-plane projection of the field, whereas the perpendicular component is represented in a blue-white-red color scale. As can be seen, the in-plane component of the field is predominantly along the direction opposite to the magnetization in Co, whereas the out-of-plane component changes from negative (blue) to positive (red) as we move from right to left in the region below the nanocontact.

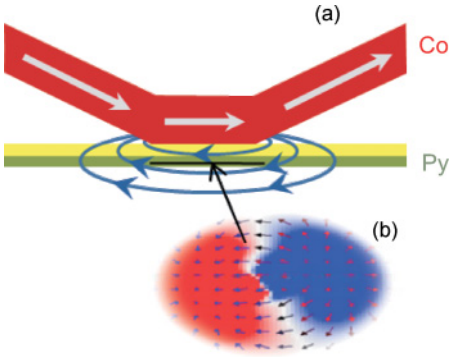

FIG. 5. (Color online) (a) Schematic representation and (b) arrow plot of the stray field created by the Co layer on the Py layer. The color scale in (b) corresponds to the perpendicular component of the stray field, where red, blue, and white mean $z > 0$, $z < 0$, and $z = 0$, respectively.

In Fig. 6(a) the sum of Oersted and stray fields in the Py layer is represented for an applied current of $I = 7.5$ mA by means of an arrow plot and a green-white-orange color scale for its module. As one can see, the stray field breaks the rotational symmetry of the Oersted field. Therefore, the position-dependent potential for the vortex is modified losing its rotational symmetry with respect to the z axis. In particular, the minimum energy position for the vortex is no longer the center of the nanocontact but it is displaced outside to the position highlighted with a red dot close to the nanocontact in Fig. 6(b). When the dynamic simulation is carried out including the ST, the vortex, initially positioned exactly at the nanocontact, is expelled from it until it reaches a stationary orbit with the frequency of $f = 380$ MHz. This orbit, plotted in Fig. 6(b), is neither circular nor symmetric with respect to the nanocontact position. As a result, the spectrum of the voltage signal is very rich in higher harmonics [Fig. 6(c)].

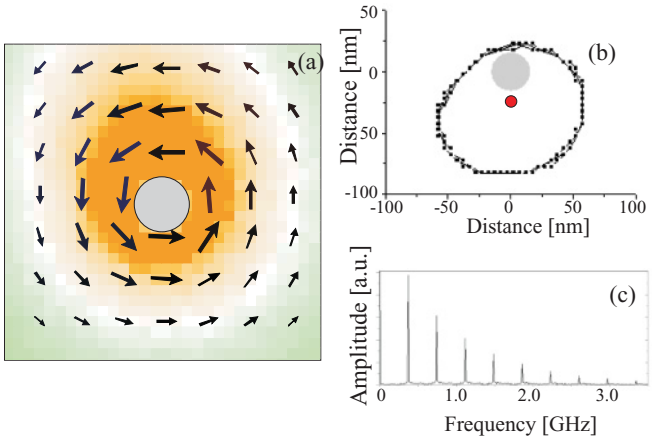

FIG. 6. (Color online) (a) Arrow plot of the sum of the Oersted ($I = 7.5$ mA) and stray fields in the vicinity of the nanocontact (highlighted in gray) in the Py layer. The strength of the total field is represented with a green-white-orange color scale. (b) Computed trajectory of the vortex core. The nanocontact is highlighted in gray, whereas the red dot indicates the equilibrium position for the vortex. (c) Frequency spectrum of the voltage signal derived from the results in (b).

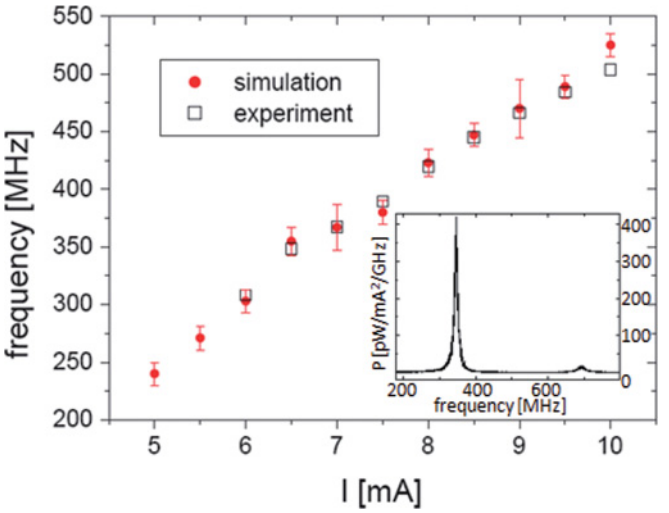

FIG. 7. (Color online) Frequency of the main peak as a function of the applied current. The results obtained from micromagnetic simulations are compared to experimental data. In the simulations, the values $\alpha = 0.009$ and $P = 0.1$ were used for the damping constant and polarizing factor, respectively. The experimental data have been obtained sweeping down the current. (Inset) An example experimental spectrum where the measured power reads 422 $pW/mA^2/GHz$ at 9 MHz linewidth.

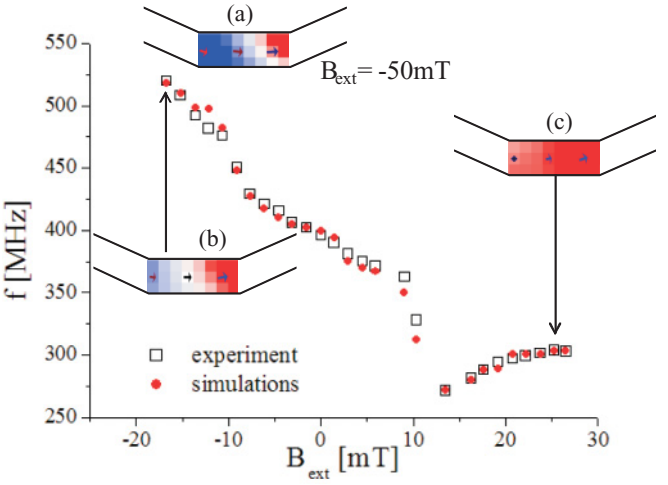

FIG. 8. (Color online) Dependence of the frequency on the strength of the out-of-plane field at the applied current $I = 7.5$ mA. In the insets the out-of-plane component of the magnetization in the Co layer is represented in a blue-white-red color scale at (a) −50 mT, (b) −17 mT, and (c) 27 mT. Both simulations and experimental data have been obtained by increasing the applied field.

Systematic simulations were carried out for different values of the applied current and similar behavior to the one described in the previous paragraph was found in all cases. The vortex behaves rigidly and it does not modify its internal structure as it circulates around the nanocontact, whereas the magnetization distribution at the nanocontact region remains magnetized mostly in-plane. The frequency of the main peak in the spectrum of the voltage signal is plotted as a function of the current and compared to experimental data in Fig. 7. The values $\alpha = 0.009$ and $P = 0.1$ were used for the damping constant and polarizing factor, respectively. The experimental data were obtained by sweeping down the current after having applied a large perpendicular field. A typical spectrum is shown in the inset of Fig. 7 where the maximum power is 422 $pW/mA^2/GHz$ and 9 MHz linewidth. Figure 7 demonstrates an excellent quantitative agreement between the simulations and the experiment. An approximately linear frequency increase with the slope of $\frac{df}{dI} = 57\ MHz/mA$ is found. Therefore, one concludes that zero-field vortex oscillations are sustained due to the combined action of the ST and the stray field, both of which are determined by the magnetization configuration in the Co layer. We emphasize the crucial role played by the stray field in this process. If this term is not taken into account in the simulations, the vortex is found to move inside the nanocontact, leading to a low-amplitude output voltage signal at much higher frequency.

IV. DYNAMIC RESPONSE TO APPLIED FIELD

In this section we first consider the sample saturated in the negative z direction and investigate the frequency response to an increasing external field at the applied current of $I = 7.5$ mA. The initial state is obtained as described Sec. III with the difference that the negative applied field favors now negative polarity of the vortex in Py. The equilibrium magnetization in the Co layer is computed for each value of the applied field. The spin polarization and the stray field acting on the Py layer are extracted from this equilibrium distribution and implemented as input for each dynamic simulation. The same parameters specified in Secs. II and III have been used here. The negative polarity of the vortex in Py is preserved throughout the studied field range. Qualitatively, the same behavior as described in Sec. III, that is, sustained vortex oscillations on a noncircular off-centered orbit, is found in all cases. As shown in Fig. 8, a nonmonotonic dependence of the frequency with the applied field is obtained, in very good quantitative agreement with the experimental data. The frequency first decreases with the external field reaching the minimum at $B_{ext} = 13.5$ mT, above which it increases. Side views of the magnetization configuration in the nanocontact region of the Co layer are presented in the insets of Fig. 8 for three different values of the external field, $B_{ext} = -50$, −17, and 27 mT, where the z component is plotted in a blue-white-red scale.

As can be observed, even at large negative fields (−50 mT), the negative (blue)-positive (red) out-of-plane profile determined by the slope of the Co layer is still present. As the strength of the negative field is reduced, this profile becomes more symmetric and the total averaged value of the stray field decreases. Consequently, the orbit gradually expands, leading to a reduction in the frequency. No change in the tendency is observed after crossing $B_{ext} = 0$ mT despite the fact that at this point the averaged out-of-plane component of the magnetization in the Co layer changes from negative to positive. This clearly indicates that in our system the perpendicular component of the spin polarization does not play a primary role in sustaining vortex oscillations. Moreover, it is observed that if the space-dependent stray field acting on Py is substituted by a uniform field of its averaged value no

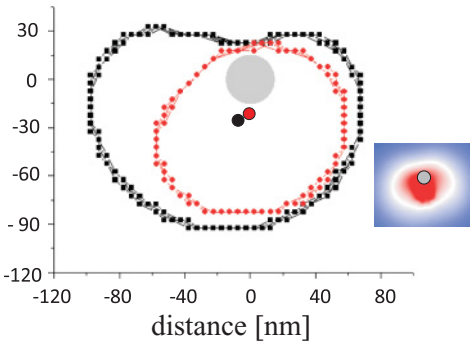

FIG. 9. (Color online) Vortex orbit at $B_{ext} = 0$ mT (red circles) and $B_{ext} = 19.9$ mT (black squares). The red and black dots represent the equilibrium position for the vortex in each case. In the inset, the magnitude of the stray field is represented in a blue-white-red scale for $B_{ext} = 19.9$ mT. The nanocontact region is marked with a gray disk in both the main panel and the inset.

oscillations are observed. Therefore, we conclude that in this low field region it is the stray field, and namely its nonuniform nature, that governs vortex oscillations.

As the strength of the positive field is increased, the negative (blue) component of the magnetization in the polarizer weakens and the configuration becomes more uniform [Fig. 8(c)]. As the negative component in Co decreases, so does the positive component of the associated stray field [Fig. 5(b)]. As a result, at the field of $B_{ext} = 13.5$ mT and above, the vortex, with negative polarity, is allowed to move further to the left of the nanocontact, leading to a more elongated orbit that closely follows the symmetry of the stray field magnitude (Fig. 9). This qualitative change in the orbit is responsible for the change of tendency in the frequency observed at $B_{ext} = 13.5$ mT. The simulations indicate that in this region the orbit slightly shrinks as the field is increased, leading to the observed frequency blueshift. Very similar behavior is obtained if the inhomogeneous character of the stray field is not accounted for, indicating that it is now the net in-plane component of the stray field that governs vortex oscillations.

Experimentally, the frequency dependence on external field varies slightly from sample to sample yielding, however, the same qualitative trends. It indicates that the feature of redshift-blueshift transition is little dependent on the small local modifications of the geometry and this result is very robust.

V. CONCLUSIONS

We have presented a numerical study of the ST-induced magnetization dynamics in a Co/Au/Py trilayer with a cone-shaped profile of the Co layer at the nanocontact region and compared it to experimental data. Calculations of the current distribution in this geometry and incorporation of the corresponding Oersted field allowed for the determination of the lowest energy configuration in the sample, defining the Py to be the active layer. Moreover, the ST-induced dynamics in this system has been shown to be governed by the formation and rotation of a magnetic vortex in the flat Py layer. These results clearly indicate that in vortex-based STNO the nucleation process depends on the exact distribution of the current-associated Oersted field, rather than on the layer thickness.

Further systematic numerical study of the frequency dependence on the current strength provided not only the qualitative explanation of the experimental observations, but also resulted in an excellent quantitative agreement between simulated and measured data. In particular, the Co-layer stray field acting on the Py layer has been demonstrated to strongly influence the magnetization dynamics. This stray field deforms the vortex orbit, resulting in the appearance of significant higher harmonics in the oscillation power spectra. Hence, vortex expulsion from the nanocontact was interpreted as a combined effect of the ST and the stray field.

Finally, the numerically obtained response to an external perpendicular field is also in excellent agreement with the experimental data. It has been shown that at low external fields, the highly inhomogeneous stray field plays a crucial role in the excitation of the vortex mode. Taking into account that this stray field comes from the locally constrained geometry of the Co layer, we claim to have observed geometry-driven vortex mode. This result demonstrates a way of tailoring spin transfer vortex oscillators by manipulating the geometry of the polarizing layer.

ACKNOWLEDGMENTS

This work was supported by EU Training Network SPINSWITCH (MRTN-CT-2006-035327), Spanish government Project No. MAT2008-04706/NAN, and Junta de Castilla y Leon Project No. SA-025A08. We acknowledge R. Guillemet, S. Fusil, K. Bouzehouane, and C. Deranlot for sample fabrication and A. Dussaux for the assistance during the measurements.

[1] J. C. Slonczewski, J. Magn. Magn. Mater. **159**, (1996).
[2] L. Berger, Phys. Rev. B **54**, 9353 (1996).
[3] D. C. Ralph and M. D. Stiles, J. Magn. Magn. Mater. **320**, 1190 (2008).
[4] J. A. Katine, F. J. Albert, R. A. Buhrman, E. B. Myers, and D. C. Ralph, Phys. Rev. Lett. **84**, 3149 (2000).
[5] S. I. Kiselev, J. C. Sankey, I. N. Krivorotov, N. C. Emley, R. J. Schoelekopf, and R. A. Buhrman, Nature (London) **425**, (2003).
[6] W. H. Rippard, M. R. Pufall, S. Kaka, S. E. Russek, and T. J. Silva, Phys. Rev. Lett. **92**, 027201 (2004).
[7] V. S. Pribiag, I. N. Krivorotov, G. D. Fuchs, P. M. Braganca, O. Ozatay, J. S. Sankey, D. C. Ralph, and R. A. Buhrman, Nat. Phys. **3**, 498 (2007).
[8] M. R. Pufall, W. H. Rippard, M. L. Schneider, and S. E. Russek, Phys. Rev. B **75**, 140404(R) (2007).
[9] Q. Mistral, M. van Kampen, G. Hrkac, J.-V. Kim, T. Devolder, P. Crozat, C. Chappert, L. Lagae, and T. Schrefl, Phys. Rev. Lett. **100**, 257201 (2008).
[10] A. Dussaux, B. Georges, J. Grollier, V. Cros, A. V. Khvalkovskiy, A. Fukushima, M. Konoto, H. Kubota, K. Yakushiji, S. Yuasa, K. A. Zvezdin, K. Ando, and A. Fert, Nat. Commun. **1**, 8 (2010).

[11] K. Yu. Guslienko, X. F. Han, D. J. Keavney, R. Divan, and S. D. Bader, Phys. Rev. Lett. **96**, 067205 (2006).
[12] K. Yu. Guslienko, B. A. Ivanov, V. Novosad, Y. Otani, H. Shima, and K. Fukamichi, J. Appl. Phys. **91**, 10 (2002).
[13] J. Shibata, Y. Nakatani, G. Tatara, H. Kohno, and Y. Otani, Phys. Rev. B **73**, 020403(R) (2006).
[14] B. A. Ivanov and C. E. Zaspel, Phys. Rev. Lett. **99**, 247208 (2007).
[15] A. V. Khvalkovskiy, J. Grollier, A. Dussaux, K. A. Zvezdin, and V. Cros, Phys. Rev. B **80**, 0140401(R) (2009).
[16] Y. S. Choi, K. S. Lee, and S. K. Kim, Phys. Rev. B **79**, 184424 (2009).
[17] G. de Loubens, A. Riegler, B. Pigeau, F. Lochner, F. Boust, K. Y. Guslienko, H. Hurdequint, L. W. Molenkamp, G. Schmidt, A. N. Slavin, V. S. Tiberkevich, N. Vukadinovic, and O. Klein, Phys. Rev. Lett. **102**, 177602 (2009).
[18] T. Devolder, J.-V. Kim, P. Crozat, C. Chappert, M. Manfrini, M. van Kampen, W. van Roy, L. Lagae, G. Hrack, and T. Schrefl, Appl. Phys. Lett. **95**, 012507 (2009).
[19] M. Manfrini, T. Devolder, J.-V. Kim, P. Crozat, N. Zerounian, C. Chappert, W. van Roy, L. Lagae, G. Hrack, and T. Schrefl, Appl. Phys. Lett. **95**, 192507 (2009).
[20] A. Ruotolo, V. Cros, B. Georges, A. Dussaux, J. Grollier, C. Deranlot, R. Guillemet, K. Bouzehouane, S. Fusil, and A. Fert, Nat. Nanotech. **4**, 528 (2009).
[21] M. Kuepferling, C. Serpico, M. Pufall, W. Rippard, T. Mitchell Wallis, A. Imtiaz, P. Krivosik, M. Pasquale, and P. Kabos, Appl. Phys. Lett. **96**, 252507 (2010).
[22] A. A. Thiele, Phys. Rev. Lett. **30**, 6 (1973).
[23] J-V. Kim and T. Devolder, e-print arXiv:1007.3859 (to be published).
[24] A. V. Khvalkovskiy, J. Grollier, N. Locatelli, Ya. V. Gorbunov, K. A. Zvezdin, and V. Cros, Appl. Phys. Lett. **96**, 212507 (2010).
[25] K. Bouzehouane, Nano Lett. **3**, 1599 (2003).
[26] Object Oriented Micromagnetic Framework (OOMMF) [http://math.nist.gov/oommf/].
[27] MAGNET-3D electromagnetic field simulation software [www.infolytica.com].
[28] K. S. Buchanan, K. Yu. Guslienko, S.-B. Choe, A. Doran, A. Scholl, S. D. Bader, and V. Novosad, J. Appl. Phys. **97**, 10H503 (2005).
[29] T. Devolder, J.-V. Kim, M. Manfrini, W. van Roy, L. Lagae, and C. Chappert, Appl. Phys. Lett. **97**, 072512 (2010).